Synthetic images by subspace transforms I. Principal components images and related filters

J. J. Sychra
University of Illinois Hospital, Department of Radiology, Room 2500, 1740 W. Taylor Street, Chicago, Illinois 60612

P. A. Bandettini
Medical College of Wisconsin, Milwaukee, Wisconsin

N. Bhattacharya and Q. Lin
University of Illinois Hospital, Department of Radiology, Room 2500, 1740 W. Taylor Street, Chicago, Illinois 60612

(Received 13 February 1992; resubmitted 13 August 1993; accepted for publication 26 October 1993)

The principal component (PC) approach offers compressions of an image sequence into fewer images and noise suppressing filters. Multiple MR images of the same tomographic slice obtained with different acquisition parameters (i.e., with different T_R,T_E, and flip angles), time sequences of images in nuclear medicine, and cardiac ultrasound image sequences are examples of such input image sets. In this paper noise relationships of original and linearly transformed image sequences in general, and specifically of original, PC, and PC-filtered images are discussed. As the spinoff, it introduces locally weighted PC transforms and filters, nonlinear PC's, and a single-image based filter for suppression of noise. Examples illustrate increased perceptibility of anatomical/functional structures in PC images and PC-filtered images, including extraction of physiological functional information by PC loading curves. Generally, the more correlated the original images are, the more effective is the PC approach.

I. INTRODUCTION

In order to obtain an MR image with the "best" description of anatomical details and/or discrimination of the tissues of interest, one may request the "optimal" pulse sequence and timing.[1–5] However, the published "optimal" parameters are rarely based on *in vivo* measurements, and when they are available for the tissue types under consideration their usefulness is limited by their variability from case to case.[6,7] Their derivation also assumes that the tissues of interest are homogeneous and that their relaxation times T_1 and T_2 are known. The determination of the optimal scanning parameters is impossible without *a priori* knowledge of the tissues and of their MR characteristics. Given the frequently exploratory character of MRI, this knowledge is often unavailable, and one may search for a lesion that was not considered when the pulse sequence was selected. Additional images obtained by varying acquisition parameters increase the probability of capturing additional diagnostic information by the resulting image set. It is important to remember that the diagnostic information may be related not only to proton density, T_1 and T_2, but also to chemical shift, signal alteration by contrast medium, degree of voxel mixing, and averaging of these parameters, stochastic properties of voxel neighborhoods (for example, multidimensional texture), flow, etc. However, this information may be difficult to extract visually, especially if the image set is composed of a large number of images, the images are noisy, mutually highly correlated, and contain overlapping structures. The images may also be difficult to view because of unwanted distributions (histograms) of pixel intensities. In another situation, a physiological process may affect only very slightly a time sequence of images, making it difficult to study this process by visual observation of the original images. In both cases, a suitable transformation of the input image set into very few (two or three) synthetic images may make the diagnostically important information more perceivable.

The synthetic images of image sequences can be separated into four main categories: (1) Functional images of a physical parameter of a physiological process, for example, time of arrival of bolus, or phase and amplitude images in cardiac nuclear medicine; (2) images of "pure" physical parameter, for example, T_1, T_2, and proton density MR images;[8] (3) the synthetic MR images that emulate original images acquired with different acquisition parameters;[9,10] and (4) images obtained by subspace methods.[11] Depending on the method used, these images can be further separated into three groups: (a) images based on unsupervised methods [for example, principal component (PC),[12–16] cluster,[12,17] and factor[12] images], (b) images derived by supervised methods (for example, eigenimages,[18–20] "maximal contrast,"[19,20] and classification images[21]); and (c) those based on the combination of these two methods (for example, "blended" images[19,20]).

It can be shown that artificial neural networks can be used to generate synthetic images similar to those produced by PC, cluster analysis, factor analysis, or discriminant analysis approach, respectively.[22,23]

Restrictions on the acquisition time often result in very noisy images. (Sequences of planar radionuclide images or sequences of cardiac ultrasound images; similarly, in an MR spin-echo image sequence that includes combinations

 0094-2405/94/21(2)/193/9/$1.20

of long and short T_Rs and T_Es, the images with long T_E and short T_R suffer disproportionally more by the noise.) *These images are usually mutually correlated, and it is therefore desirable to exploit the presence of the common information to increase their signal-to-noise ratio (S/N) and/or to transform them into a smaller set of uncorrelated images without a significant loss of information.* In this paper, we discuss the PC approach toward these two goals and add to the previous studies[12–15,19,24,25] the noise analysis in synthetic images produced by linear transform, in general, and by PC transform, in particular (one has to acknowledge the detail analysis[26] of error propagation in eigenimages by Soltanian-Zadeh *et al.*). Further, we introduce nonlinear, locally weighted, and single image based PC transforms and filters, respectively (see Appendix B). Results are illustrated by examples taken from MRI and nuclear medicine.

II. NOISE PROPAGATION BY LINEAR TRANSFORMS OF IMAGE SEQUENCES

A. The image transform

Let $\{\mathcal{F}\}=[\mathcal{F}(1),\mathcal{F}(2),...,\mathcal{F}(n)]$ be the set of acquired image matrices $\mathcal{F}(k)$ of the same view or of the same tomographic slice. The vector $\mathbf{w}_{xy}=[\mathcal{F}(1)_{xy},\mathcal{F}(2)_{xy},...,\mathcal{F}(n)_{xy}]^T$ is the input pixel intensity vector at column x and row y. The pixel intensity p in the synthetic image obtained by a linear transform is

$$p(\mathbf{w})=\Sigma e_i w_i+s=\mathbf{e}^T\mathbf{w}+s, \tag{1}$$

where s is usually determined by display requirements (assume $s=0$ unless specified otherwise). We distinguish the pixel intensity p from the actual display brightness, which is a function of $p(\mathbf{w})$ and is determined by the display hardware and by the operator. Without a loss of generality, we assume

$$\mathbf{e}^T\mathbf{e}=1. \tag{2}$$

The synthetic pixel intensity is then given by the projection of the signal vector $\mathbf{w}$ on the unit transformation vector $\mathbf{e}$.

The relations derived in this section are applicable to (1) principal component images,[11–15,19,20] (2) factor analysis images,[13,15,27,28] (3) discriminant function images obtained either by the normal mixture cluster analysis[15,17,19,20] or by the discriminant analysis,[15] (4) eigenimages,[18–20] and to (5) maximum contrast images,[19,20] as they are all examples of images generated by linear transforms (1).

B. The noise of the input image

Let us assume that the signal vector $\mathbf{w}$ has a deterministic component $\mathbf{r}$ and a random noise component $\mathbf{h}$:

$$\mathbf{w}=\mathbf{r}+\mathbf{h}. \tag{3}$$

We will consider two types of signal averaging: (1) the *local* mean over "unlimited" and independent repetitions of a measurement of the pixel intensity ($\langle\ \rangle_{RM}$); and (2) the *sample* mean over the spatial region of interest (ROI,$\langle\ \rangle_{ROI}$). When both averagings take place (the *global* mean) we use notation $\langle\langle\ \rangle\rangle$. The first type yields an estimate of a local "expected value," and the second one provides a mean over a finite number of pixels of a single acquisition. We assume that the signal noise is additive and uncorrelated, and with zero mean:

$$\begin{aligned}&\langle\mathbf{h}\rangle_{RM}=0,\\ &\langle h_i h_j\rangle_{RM}=\delta_{ij}\langle h_i^2\rangle_{RM},\\ &\mathbf{\Sigma}_h\equiv\langle\mathbf{h}\mathbf{h}^T\rangle_{RM}.\end{aligned} \tag{4}$$

We will discuss two noise models in detail and demarcate them by offset text blocks in italics.

The noise of the first kind is characterized by

$$\mathbf{\Sigma}_h=\sigma_h^2\mathbf{I}, \tag{5}$$

where $\mathbf{I}$ *is the (n,n) identity matrix. The* MR *spine-echo image set*[1–4] *can be used as an example of this kind of noise [when using images with different* T_R *and* T_S*, the pixel intensities of input images should be scaled first by a factor proportional to* (T_S/T_R)*]. In radionuclide images the noise follows the Poisson statistics (the noise of the second kind):*

$$(\mathbf{\Sigma}_h)_{ii}=r_i. \tag{6}$$

To bypass the problems of the observer's perception of contrast and the properties of the display, we will study the contrast in the space of the original and synthetic signals.

The global covariance matrices of the input pixel intensities and their components are defined by

$$\begin{aligned}(\mathbf{\Sigma}_I)_{ij}&\equiv\langle\langle(w_i-\langle\langle w_i\rangle\rangle)(w_j-\langle\langle w_j\rangle\rangle)\rangle\rangle\\ &=\langle\langle(w_i-\langle r_i\rangle_{ROI})(w_j-\langle r_j\rangle_{ROI})\rangle\rangle,\\ (\mathbf{\Sigma}_M)_{ij}&\equiv\langle\langle(r_i-\langle\langle r_i\rangle\rangle)(r_j-\langle\langle r_j\rangle\rangle)\rangle\rangle\\ &=\langle(r_i-\langle r_i\rangle_{ROI})(r_j-\langle r_j\rangle_{ROI})\rangle_{ROI},\\ (\mathbf{\Sigma}_N)_{ij}&\equiv\langle\langle(h_i-\langle\langle h_i\rangle\rangle)(h_j-\langle\langle h_j\rangle\rangle)\rangle\rangle=\langle(\mathbf{\Sigma}_h)_{ij}\rangle_{ROI},\end{aligned} \tag{7}$$

where $i,j=1,2,...,n$. Obviously,

$$\mathbf{\Sigma}_I=\mathbf{\Sigma}_M+\mathbf{\Sigma}_N. \tag{8}$$

In the case of *the noise of the first kind,*

$$\mathbf{\Sigma}_N=\sigma_h^2\mathbf{I}, \tag{9}$$

and in the case of *the noise of the second kind,*

$$(\mathbf{\Sigma}_N)_{ij}=\delta_{ij}\langle\langle w_i\rangle\rangle=\delta_{ij}\langle r_i\rangle_{ROI}. \tag{10}$$

(The global variance of the components of the pixel intensities in the kth input image are the diagonal elements,

$$\sigma_{w,k}^2\equiv(\mathbf{\Sigma}_I)_{kk},\quad \sigma_{r,k}^2\equiv(\mathbf{\Sigma}_M)_{kk},\quad \sigma_{h,k}^2\equiv(\mathbf{\Sigma}_N)_{kk}. \tag{11}$$

The standard deviation $\sigma_{r,k}$ can be used as the measure of the "global contrast" in the kth input image, and $\sigma_{r,k}/\sigma_{h,k}$ as the measure of C/N. These measures can be evaluated using (8): the signal variance $\sigma_{w,k}^2$ can be estimated from (7) and the noise variance $\sigma_{h,k}^2$ can be estimated, for example, by the analysis of variance (ANOVA) on input image sets acquired by repeated acquisitions.

However, in the case of the noise of the first kind a more practical way is to estimate $\sigma_{h,k}^2$ *from pixel intensities* [3]

outside the scanned body (air or a homogeneous object scanned together with the patient). In the case of the noise of the second kind,

$$\sigma_{h,k}^2=\langle\langle w_k\rangle\rangle\approx\langle w_k\rangle_{\mathrm{ROI}}. \tag{12}$$

C. The noise of the synthetic image

The local variance σ_p^2 of pixel intensity in the synthetic image is

$$\sigma_p^2=\langle(p(\mathbf{w})-\langle p(\mathbf{w})\rangle_{\mathrm{RM}})^2\rangle_{\mathrm{RM}}. \tag{13}$$

After simplification by (1), (3), and (4),

$$\sigma_p^2=\langle(\mathbf{e}^T\mathbf{h})^2\rangle_{\mathrm{RM}}, \tag{14}$$

i.e.,

$$\sigma_p^2=\sum_{i=1}^{n} e_i^2(\Sigma_h)_{ii}. \tag{15}$$

In the case of the noise of the first kind, (15) reduces to

$$\sigma_p^2=\sigma_h^2, \tag{16}$$

i.e., the noise variances in the synthetic and original images are the same, and in the case of the noise of the second kind,

$$\sigma_p^2=\Sigma e_i^2 r_i. \tag{17}$$

The global standard deviations of the synthetic signal and of its deterministic and noise components, respectively, are

$$\sigma^2{}_I=\mathbf{e}^T\boldsymbol{\Sigma}_I\mathbf{e},\quad \sigma^2{}_M=\mathbf{e}^T\boldsymbol{\Sigma}_M\mathbf{e},\quad \sigma^2{}_N=\mathbf{e}^T\boldsymbol{\Sigma}_N\mathbf{e}, \tag{18}$$

and are mutually related by

$$\sigma_I^2=\sigma_M^2+\sigma_N^2. \tag{19}$$

From (2), (4), (7), and (18) it follows that the extreme noise variances of input and synthetic images are the same:

$$\begin{aligned}&\max_{(e)}\sigma^2{}_N=\max_{(i)}\langle\langle h_i^2\rangle\rangle,\\ &\min_{(e)}\sigma^2{}_N=\min_{(i)}\langle\langle h_i^2\rangle\rangle.\end{aligned} \tag{20}$$

From the definition of principal components (see below), it follows that the smallest eigenvalue λ_n of the covariance matrix of the input pixel intensities is the smallest possible variance of the synthetic signal:

$$\lambda_n=\min_{(e)}\langle[p(\mathbf{w})-\langle p(\mathbf{w})\rangle_{\mathrm{ROI}}]^2\rangle_{\mathrm{ROI}}. \tag{21}$$

From (19) to (21), it follows that the smallest expected eigenvalue can be used as an upper estimate of the noise variance σ_N^2:

$$\langle\lambda_n\rangle_{\mathrm{RM}}=\min_{(e)}\langle\sigma_p^2\rangle_{\mathrm{ROI}}\geqslant\sigma_N^2=\mathbf{e}_n{}^T\boldsymbol{\Sigma}_N\mathbf{e}_n\geqslant\min_{(e)}\sigma_N^2. \tag{22}$$

In the case of the noise of the first kind the noise variance does not depend on the transformation vector **e** *and*

$$\langle\lambda_n\rangle_{\mathrm{RM}}\geqslant\sigma_N^2=\sigma_h^2. \tag{23}$$

Usually, the eigenvalue λ_n is close to the expected eigenvalue $\langle\lambda_n\rangle_{\mathrm{RM}}$ and may be used to replace it in (22) and (23), and often

$$\langle\lambda_n\rangle_{\mathrm{RM}}\approx\min_{(e)}\sigma_I^2. \tag{24}$$

D. The contrast of the synthetic image

The relations derived above can be used to compare contrast (and C/N) of original and synthetic images.

For example, in the case of noise of the first kind the ratio

$$\sigma_M/\sigma_{r,k}\equiv(\sigma_M/\sigma_N)/(\sigma_{r,k}/\sigma_N) \tag{25}$$

becomes

$$\begin{aligned}\sigma_M/\sigma_{r,k}&\equiv(\sigma_M/\sigma_N)/(\sigma_{r,k}/\sigma_N)\\ &=[(\mathbf{e}^T\boldsymbol{\Sigma}_I\mathbf{e}-\sigma_h^2)/(\sigma_{w,k}^2-\sigma_h^2)]^{1/2},\end{aligned} \tag{26}$$

and satisfies the inequality

$$\begin{aligned}(\mathbf{e}^T\boldsymbol{\Sigma}_I\mathbf{e}/\sigma_{w,k}^2)^{1/2}\lesseqgtr\sigma_M/\sigma_{r,k}\lesseqgtr[(\mathbf{e}^T\boldsymbol{\Sigma}_I\mathbf{e}-\lambda_n)/\\ (\sigma_{w,k}^2-\lambda_n)]^{1/2},\end{aligned} \tag{27}$$

for $\mathbf{e}^T\boldsymbol{\Sigma}_I\mathbf{e}\lesseqgtr\sigma_{w,k}^2$. *The difference of the global contrasts of the synthetic image and of the kth original image is easier to calculate and does not require the knowledge of noise variances:*

$$\sigma_M^2-\sigma_{r,k}^2=\mathbf{e}^T\boldsymbol{\Sigma}_I\mathbf{e}-\sigma_{w,k}^2. \tag{28}$$

However, this is not true in the case of the noise of the second kind:

$$\sigma_M^2-\sigma_{r,k}^2=\mathbf{e}^T\boldsymbol{\Sigma}_I\mathbf{e}-\sigma_{w,k}^2+\langle r_k\rangle_{\mathrm{ROI}}-\Sigma e_i^2\langle r_i\rangle_{\mathrm{ROI}}. \tag{29}$$

Usually one may substitute

$$\langle r_i\rangle_{\mathrm{ROI}}\approx\langle w_i\rangle_{\mathrm{ROI}}, \tag{30}$$

and the difference of the contrasts can be calculated directly from the input images and the transformation vector **e**.

III. PRINCIPAL COMPONENT IMAGES

For simplicity, let us assume that there is only one unit transformation vector $\mathbf{e}_1$ that results in a synthetic image with maximal variance,

$$\lambda_1=\max_{\mathbf{e}_1}\langle(p(\mathbf{w})-\langle p(\mathbf{w})\rangle_{\mathrm{ROI}})^2\rangle_{\mathrm{ROI}} \tag{31}$$

(disregard the obvious opposite-sign solution $-\mathbf{e}_1$).

In the case of the noise of the first kind, S/N *in this synthetic image is obviously greater or equal to* S/N *of any of the input images, and one intuitively expects a greater information content as well. This inequality is not guaranteed in the case of the noise of the second kind, however, we have never observed its violation in clinical data.*

The image transformation process may be expanded by searching for the transformation vector $\mathbf{e}_2$ in the $(n-1)$-dimensional subspace that is orthogonal to the vector $\mathbf{e}_1$, and so on, ..., until all n transformation vectors are found. This may be viewed as a rotation of the original coordinate system into a new one with axes parallel to $\{\mathbf{e}_1,\mathbf{e}_2,\mathbf{e}_3,\ldots,\mathbf{e}_n\}$, and yielding the corresponding synthetic image set. Usually the input images are strongly correlated, and consequently the last images of this new set are extremely

noisy, their variances of pixel intensities tend to be only slightly higher than the noise variance σ^2_N and contain very little or no useful information. Consequently, the original image set can be replaced by the smaller set of the first few synthetic images without a significant loss of information.

The process described above is known as the principal component analysis,[11,16,29,30] the transformation vectors $\mathbf{e}_i$, $i=1,2,...,n$, are the eigenvectors of the covariance matrix of the input pixel intensities (calculated over the ROI sample), and the eigenvalues λ_i are the corresponding variances of the PCs. They are related to the signal variance by

$$\sigma_I^2|_{e_i}=\langle\lambda_i\rangle_{\mathrm{RM}}\approx\lambda_i. \tag{32}$$

In the case of the noise of the first kind the expression for global C/N in the ith PC *image reduces to*

$$\sigma_M/\sigma_N=[(\langle\lambda_i\rangle_{\mathrm{RM}}/\sigma_h^2)-1]^{1/2} \geqslant[(\langle\lambda_i\rangle_{\mathrm{RM}}/\langle\lambda_n\rangle_{\mathrm{RM}})-1]^{1/2}. \tag{33}$$

The PC image transform can be implemented in the following steps.

(1) Define the input data: Example: PC MRI images of the brain. Select the input image set (for example, eight spin-echo images of a tomographic slice: TR=500, 2000 ms, TE=20, 40, 60, and 80 ms), and the pixels (ROI) whose intensities $\mathbf{w}$ will be used to derive the PC analysis transform. Pixels outside the brain are of no interest, and their presence in the ROI is usually undesirable, as they may influence the PC transform at the expense of the brain data. The ROI does not have to contain all brain pixels: often enhanced structures of a brain subregion can be obtained by choosing this subregion as the ROI.

(2) Compute the covariance matrix $\mathbf{C}$,

$$\mathbf{C}_{ij}=\langle(w_i-\langle w_i\rangle_{\mathrm{ROI}})(w_j-\langle w_j\rangle_{\mathrm{ROI}})\rangle_{\mathrm{ROI}}, \quad i,j=1,2,...,n, \tag{34}$$

and its eigenvalues λ_i and eigenvectors $\mathbf{e}_i$.

(3) Use (1) to compute the pixels' PC values and generate the corresponding PC images.

How many PC images should be calculated and retained? What is the "essential" dimensionality of data? There is no simple and agreed on answer.[29] We believe that a number of criteria should be used in a combination: First, we may reject the PC's with eigenvalues lower than a specified fraction of the first eigenvalue λ_1. In the example above, $\sqrt{(\lambda_n/\lambda_1)}=0.05$ is often a good threshold choice, but may be too high in case of brain activation studies (see Sec. V and Fig. 2). A similar condition can be applied to the ratio of the PCs eigenvalues and to the sum of all n eigenvalues. Further, the cutoff point can be determined by "eyeballing" a curve fitted through points $[i,\sqrt{\lambda_i}]$, $i=1,2,...,n$ and by finding where the curve "levels off." Karny and Samal[31] have recently proposed a Bayesian estimate of the number of significant PCs. While this estimate is often very good, it is our opinion that it is safer to use it as a low estimate. Ultimately, one can calculate and display all PC images and reject those that seem to contain practically only noise.

The PC version of (1) can be written in matrix notation ($s=0$),

$$\mathbf{p}=\mathbf{E}\mathbf{w}, \tag{35}$$

where $\mathbf{p}=[p_1,p_2,...,p_n]^T$ is the PC pixel intensity vector. The eigenmatrix $\mathbf{E}=[e_{ij}]$ is orthonormal, its rows are eigenvectors, and its transpose is its inverse,

$$\mathbf{E}^T=[\mathbf{e}_1{}^T,\mathbf{e}_2{}^T,...,\mathbf{e}_n{}^T]=\mathbf{E}^{-1}, \tag{36}$$

and the PCs are mutually uncorrelated:

$$\langle(p_i-\langle p_i\rangle_{\mathrm{ROI}})(p_j-\langle p_j\rangle_{\mathrm{ROI}})\rangle_{\mathrm{ROI}}=\delta_{ij}\lambda_j, \quad i,j=1,2,...n. \tag{37}$$

Examples of PC images are presented in Sec. V. Some extensions of this approach are briefly outlined in Appendix B.

IV. NOISE SUPPRESSION BY PC-BASED FILTER

A. The PC filter

From (35) and (36), it follows that the original images can be obtained from their principal components by the inverse transform

$$\mathbf{w}=\mathbf{E}^T\mathbf{p}. \tag{38}$$

Let us assume that the input images are mutually correlated and that the last $n-m$, $1<m<n$, PC components contain practically only noise. Their contribution in the inverse transform (38) can be eliminated by setting

$$p_j=0, \quad \text{for } m<j\leqslant n. \tag{39}$$

From (35), (38), and (39), it follows that the resulting filtered pixel intensity $\mathbf{w}'_i$ in the ith image can be written as

$$\mathbf{w}'=\mathbf{F}\mathbf{w}, \quad \text{or} \quad \mathbf{w}'=\mathbf{w}-\mathbf{\Phi}\mathbf{w}, \tag{40}$$

where the filter $\mathbf{F}$ and its supplement $\mathbf{\Phi}=\mathbf{I}-\mathbf{F}$ are given by

$$F_{ij}=\sum_{k=1}^{m}e_{ki}e_{kj}, \quad i,j=1,2,...,n, \qquad \Phi_{ij}=\delta_{ij}-F_{ij}=\sum_{k=m+1}^{n}e_{ki}e_{kj}. \tag{41}$$

B. The noise in the PC-filtered images

In analogy to (3), let us separate the deterministic and noise parts of the filtered intensities,

$$\mathbf{w}'=\mathbf{r}'+\mathbf{h}'. \tag{42}$$

From (40) and (42), it follows that

$$\mathbf{h}'=\mathbf{F}\mathbf{h}, \tag{43}$$

$$\mathbf{r}'=\mathbf{F}\mathbf{r}; \tag{44}$$

one can obtain the relationship between the noise in the filtered and original images from (5), (7), and (42):

$$\langle h_i'^2\rangle_{\mathrm{RM}} = \sum_{j=1}^{n} F_{ij}^2 \langle h_j^2\rangle_{\mathrm{RM}}, \tag{45}$$

$$\langle\langle h'^2_i\rangle\rangle = \sum_{j=1}^{n} F_{ij}^2 \sigma_{h,j}^2. \tag{46}$$

From the definition (41) of the filter **F** *and from the orthonormality of the eigenmatrix* **E**, *it follows that in the case of the noise of the first kind, expressions (45) and (46) can be reduced to*

$$\langle h_i'^2\rangle_{\mathrm{RM}} = \langle\langle h_i'^2\rangle\rangle = \langle h^2\rangle_{\mathrm{RM}} \sum_{k=1}^{m} e_{ki}^2 \left[= \langle h^2\rangle_{\mathrm{RM}} \left(1 - \sum_{k=m+1}^{m} e_{ki}^2\right)\right]. \tag{47}$$

In the case of the noise of the second kind, (45) and (46) become

$$\langle h_i'^2\rangle_{\mathrm{RM}} = \sum_{j=1}^{n} F_{ij}^2 r_j, \tag{48}$$

$$\langle\langle h_i'^2\rangle\rangle \approx \sum_{j=1}^{n} f_{ij}^2 w_j, \tag{49}$$

respectively.

One may notice that Eq. (47) includes, as a special case, the noise decrease by averaging n images that differ only by the noise content. In such a case only the first PC is meaningful ($m=1$), and all components of the first eigenvector are equal to $n^{-1/2}$, and consequently the ratio $\langle h_i'^2\rangle_{\mathrm{RM}}/\langle h^2\rangle_{\mathrm{RM}}$ becomes $1/n$, as expected.

C. The bias in the PC-filtered images

From (41) and (44), it follows that

$$r'_i = r_i - \sum_{j=1}^{n} \Phi_{ij} r_j = r_i - \sum_{s=m+1}^{n} e_{si}\rho_s, \quad i=1,2,\ldots,n, \tag{50}$$

where the sum represents the bias caused by the rejection of the last $(n-m)$ PCs, and ρ_s are the discarded deterministic components of PCs:

$$\mathbf{r} = \mathbf{E}^T\boldsymbol{\rho}. \tag{51}$$

If a filtered image sequence is used as an input for a quantitative analysis, for example, functional studies in nuclear medicine, it is imperative that only negligible information is discarded. One may visually examine differential images ($\mathbf{w}'-\mathbf{w}$) together with the last $(n-m)$ PC images, to verify that they do not contain any significant information. One can also compensate for the mean bias and for the mean difference of the contrast by the corresponding shift and scaling of the filtered pixel values, respectively. However, we have found these corrections to be rarely needed: in planar radionuclide image sequences of a kidney the mean bias amounted to less than 2% of the mean pixel intensities, and in the case with the eight spin-echo MR images the mean bias was less than 3%.

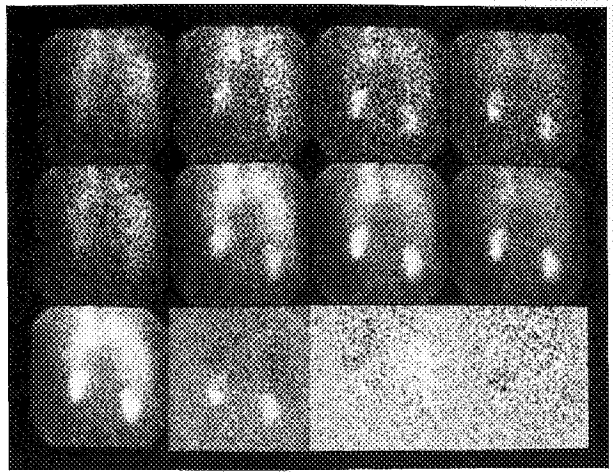

FIG. 1. Nuclear medicine: a renal study. First row: First, fourth, eighth, and twelfth input images of a 14 image set; second row: the corresponding filtered images (based on four PCs; third row: the first four PC images.

Let us look, in a simplified manner, at the PC filter in extreme situations. First, let the ith original image differ very much from the rest of the input image set, more accurately, let $|(\Sigma_M)_{ij}| \ll (\Sigma_M)_{ii}$, $j=1,2,\ldots,i-1,i+1,\ldots,n$. In such a case there is a PC image that resembles very much the ith image, as it will contain very little contribution from other images. If the PC is selected for the construction of the filter, the noise in the filtered version of the ith image will be suppressed very little, and if too few PCs are selected, a noticeable amount of "alien" information "seeps" from the ith image into filtered versions of other images. If the PC is not selected, the "filtered" version of the ith image is a failure, because it does not resemble the original image (the significantly lower noise in the resulting image can hardly be a source of satisfaction...). On the other side, if there is a large subset of input images that are very similar (that are mutually highly correlated), there is probably a PC that represents these images much more than any other PC. If this PC is selected for the filter construction, the noise in the filtered versions of the image subset will be significantly suppressed. However, if the PC is not selected—which is unlikely—the filtering is not successful, as the filtered versions of image subsets are mainly combinations of the remaining input images.

V. EXAMPLES

The first example (Fig. 1) is a case of a dynamic radionuclide kidney study. The first row contains the first, fourth, eighth, and twelfth input images of a 14-image input sequence, respectively. The second row holds the corresponding filtered images calculated from the first four PCs. The third row contains the corresponding four PC images. The first four PCs contain most of the information and it can also be seen from the sequence of the relative standard deviations $\sqrt{(\lambda_i/\lambda_1)}$, which are for $i=2$, 3, 4, and 14 equal to 0.407, 0.288, 0.263, and 0.215, respectively.

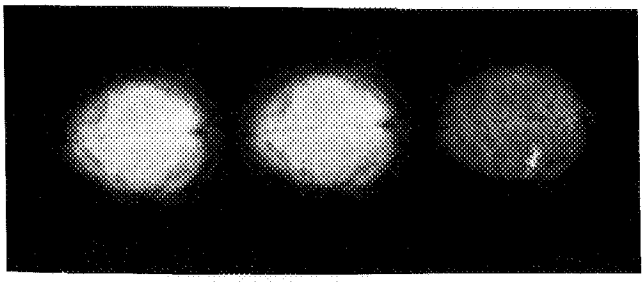

FIG. 2. MRI: activation of the motor cortex. Selected two input images out of 122 (acquired at time 57 and 64 s, respectively), originally, 64×64 pixels each, EPI on 1.5 T GE Signa scanner, TR=1000 ms and TE=40 ms. The third image is the second PC image.

This is confirmed by the fact that the first four PCs contain 68% of the total signal variance (approximately 9.5% is noise and 58.5% is deterministic), and the remaining PCs contain 32% (approximately 23.6% is noise and 8.4% is deterministic). The noise is responsible for at least 33% of the total signal variance. (As we deal with noise of the second kind, these are actually the low estimates of the noise component based on the value of the last eigenvalue, and the high estimates of the deterministic component of the total signal variance, respectively.) The filtered images demonstrate a significant increase of S/N and better delineation of the kidneys. The first few original images (at the beginning of the radionuclide uptake) differ very much from the following images, and consequently their filtered versions show relatively smaller increase of S/N (see the first image in the second row).

The second example is a case of MRI brain activation (Fig. 2): a normal subject moved and then rested the finger for a total of 25 s, and repeated this process several times. The input image set consists of 122 EPI images acquired one second apart. While the MRI signal increases as a result of the decrease of concentration of deoxyhemoglobin,[32] the effect of activation is masked by the noise and is practically impossible to detect in the original images visually. Two input images have been selected to illustrate this point: they were acquired at time 57 and 64 s, respectively, and should show best the difference corresponding to the activation (they correspond to opposite local extreme values of the loading curve; see below). However, the second PC image successfully extracts the effect of activation. When the whole image ROI is used, $\sqrt{(\lambda_2/\lambda_1)}=0.010$. To improve the extraction of the activation effect, a smaller ROI centered at the activation domain has been used and yielded $\sqrt{(\lambda_2/\lambda_1)}=0.038$. The corresponding PC image is displayed as the last image in Fig. 2, and indicates clearly the location of the activated motor cortex. The corresponding eigenvector is represented by the loading curve in Fig. 3, and its periodic maxima (25 s apart) correspond to the activation. As we can see, the eigenvectors are helpful, not only for the construction of PC images but also for the description of data structures, in this case, of a physiological process. As the application of the PC approach is practically independent on the knowledge of how the activation was administered, it offers an alternative[32] investigative and imaging tool. We will discuss use of this technique for the detection, analysis, and imaging of brain activation in detail in a separate communication.

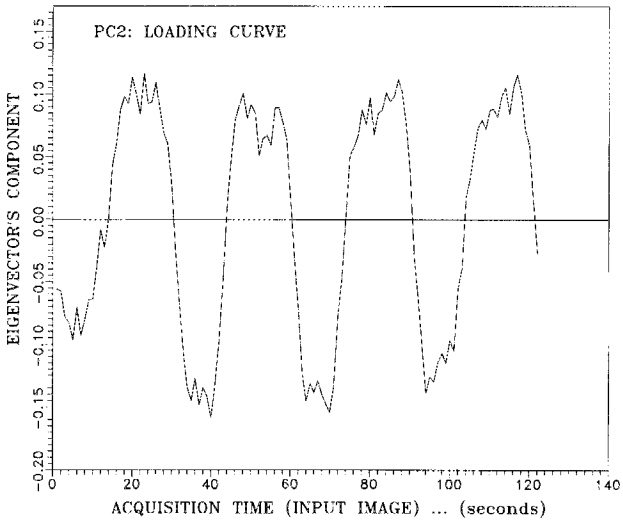

FIG. 3. MRI: activation of the motor cortex. The loading curve of the corresponding second PC (components of the second eigenvector)—see Fig. 2. The maxima—about every 25 s—are associated with the motor cortex activation (finger movement).

VI. CONCLUSIONS

We have derived statistical expressions for the propagation of noise from the original images into linear synthetic images, and then studied these relationships in more detail in the special case of PC images and for two noise models that are applicable in nuclear medicine and MRI, respectively. As a spinoff, we have derived a statistical expression for the relationship between contrast in the original and PC images. Further, we have derived statistical expressions for the noise in PC-filtered images as a function of the filter and of the original noise, followed by the expression for bias of PC-filtered images.

Principal component analysis applied to a sequence of mutually correlated images provides image data compression and offers noise suppressing filters. The resulting first few PC images often possess a greater S/N, and the image data structure can be perceived easier and in a small number of images. Usually, the first PC image is an "average" of the input images, and the next few PC images represent their "differences." As the PC transform depends on the input data (i.e., on the studied case), the PC images are not always easy to compare from case to case. Consequently, their value is mainly exploratory. When a fixed acquisition protocol is used, a pseudo-PC transform that is independent of individual cases may be derived (Appendix B), and the resulting pseudo-PC images may replace the original images in clinical applications.

The PC-filtered images do not suffer by spatial blurring, which is typical to low pass, noise suppressing filters that are based on a single image. The comparison of eigenvalues of the used and of the discarded PCs usually helps to eval-

uate the tradeoff between the noise removal and information loss by the PC filter. In a simplified way, the more the input images are mutually correlated, the greater noise suppression is achieved by the PC filter: the more an input image is "different" from other input images, the less its noise will be suppressed by the PC filter (see the first image in the second row of Fig. 1). Also, the smaller the number of PCs selected to build the filter, the more will be noise suppressed in filtered images and more of the "wrong information" may "seep" from other input images into a filtered image.

A PC filter based on a single image (Appendix B) offers a controlled removal of noise without the explicit need to know the noise spectrum. Its relationship to traditional "optimal" filters is under investigation.

ACKNOWLEDGMENTS

This work was supported by GE Medical Systems and by a research grant from the Chicago Chapter of the Cancer Society. The authors are grateful to Dr. D. Pavel for image data and comments on the PC filter in nuclear medicine, and to Dr. Riederer and Dr. Farzaneh for the composite spin-echo pulse sequence program.

APPENDIX A: STOCHASTIC TRANSFORMATION VECTOR e

In the text above, we have assumed that the transformation vector $\mathbf{e}$ is well known. However, as $\mathbf{e}$ is often derived from sampled noisy image data, it may have a stochastic nature. For simplicity, it is fair to assume that the noise component $\mathbf{h}$ of signal $\mathbf{w}$ and noise component $\boldsymbol{\epsilon}$ of $\mathbf{e}$ satisfy the following conditions:

$$\mathbf{e}=\mathbf{e}_0+\boldsymbol{\epsilon}, \tag{A1}$$

$$\langle \epsilon_i \epsilon_j \rangle_{\mathrm{RM}}=\delta_{ij}\sigma_{e,i}{}^2, \tag{A2}$$

$$\langle h_i \epsilon_j \rangle_{\mathrm{RM}}=0, \tag{A3}$$

$$\langle h_i h_j \epsilon_k \rangle_{\mathrm{RM}}=0, \tag{A4}$$

$$\langle h_i h_j \epsilon_i \epsilon_j \rangle_{\mathrm{RM}}=\delta_{ij}(\Sigma_h)_{ii}\sigma_{e,i}{}^2, \tag{A5}$$

where $\mathbf{e}_0$ is the deterministic part of $\mathbf{e}$ and $\sigma_{e,i}{}^2$ is the variance of ϵ_i. Then Eqs. (16) and (20) should be modified accordingly:

$$\begin{aligned}\sigma_p{}^2 &= \langle (p(\mathbf{w})-\langle p(\mathbf{w})\rangle)^2\rangle_{\mathrm{RM}} \\ &= \langle (\mathbf{ew}-\mathbf{e}_0\mathbf{r})2\rangle_{\mathrm{RM}} \\ &= \sum_{i=1}^{n} (e_{0i}{}^2+\sigma_{e,i}{}^2)(\Sigma_h)_{ii}+\sum_{i=1}^{n} r_i{}^2\sigma_{e,i}{}^2, \end{aligned} \tag{A6}$$

$$\sigma^2{}_I=\mathbf{e}^T\boldsymbol{\Sigma}_I\mathbf{e}+\sum_{i=1}^{n}\langle\langle w_i{}^2\rangle\rangle\sigma_{e,i}{}^2,$$

$$\sigma^2{}_M=\mathbf{e}^T\boldsymbol{\Sigma}_M\mathbf{e}+\sum_{i=1}\langle r_i{}^2\rangle_{\mathrm{ROI}}\sigma_{e,i}{}^2, \tag{A7}$$

$$\sigma^2{}_N=\mathbf{e}^T\boldsymbol{\Sigma}_N\mathbf{e}+\sum_{i=1}\langle\langle h_i{}^2\rangle\rangle\sigma_{e,i}{}^2.$$

If needed, other relations in the paper may be modified in the same manner.

APPENDIX B: POSSIBLE EXTENSIONS OF THE PC APPROACH

1. Nonlinear principal component images

It is sometimes advantageous to apply PC transform to an MR image set that includes nonlinear transformations, for example, products of the original images. The resulting PC images often possess a greater contrast between tissue types and reveal structures that are difficult to detect in the original images or linear PC images. However, the correct interpretation of these images is usually more difficult. The noise propagation analysis is much more complex and yields nonlinear bias terms.[20]

2. Locally sensitive PC transform and filter

We have assumed so far that the PC transform and filter are defined on a "global" ROI, possibly on the whole image. The "local" PC and PC-filtered values are then influenced by "distant" image structures (pixel intensity vectors). If these distant structures differ significantly from the local one (i.e., the contribution of the distant structures to the covariance matrix is significantly different than the contribution of the local structure), the calculated "local" PC and PC-filtered values become less sensitive to a local image structure. To represent local structure adequately the "minimal" PC set may be larger than in the case of insignificantly different distant structures. When this insensitivity becomes an important drawback, a corrective technique is needed. The result in "PC" definition changes from pixel to pixel and comparison of PC values in mutually distant pixels may become difficult if not impossible. Currently, we are studying corresponding techniques based (1) on an iterative solution of the eigenproblem with locally perturbed covariance matrix, and (2) on conditional interpolation of eigenvectors calculated on a sparse lattice, respectively.

A simpler approach is to select a suitable, smaller ROI that includes the structures of interest. This process is relatively fast and the obtained PC images are usually more informative in the ROI domain. In addition, they may be used to search for similar structures in the rest of the image (a PC loading curve is used as a "match filter").

3. Pseudoprincipal component images

We have observed in brain spin-echo input image sets of $T_R=2$ s and $T_E=20$, 40, 60, and 80 ms, respectively, the first PC image to be usually very close to the average of the input images,

$$\mathbf{e}_1\approx[0.5,0.5,0.5,0.5]^T, \tag{B1}$$

and the second PC image to be a "difference" of the four input images,

$$\mathbf{e}_2\approx[-3/\sqrt{20},-1/\sqrt{20},1/\sqrt{20},3/\sqrt{20}]^T. \tag{B2}$$

(This input image set has the advantage of containing more information than the usually used clinical set, with TR=2 s, TE=20 and 80 ms, respectively, but requires about the same acquisition time.) The third PC image often contains only a rough silhouette of the head and noise, and is usually diagnostically useless. In our experience, this is consistently true for the fourth PC image. Consequently, one may propose pseudo-PC synthetic images based on (1), (B1), and (B2). The transform is simple, fast, and independent of the studied case (it provides standardized synthetic images that permit a direct comparison of individual cases). The first pseudo-PC image has significantly better S/N and the second pseudo-PC image has much better tissue related contrast than the original images. Our experience indicates that similar pseudoeigenvectors may be found for other clinical situations and combinations of T_R and T_E.

4. PC filter based on a single image

A PC filter may be applied to a single image in a way reminiscent of an early approach of DiPaola[24] and Schmidlin.[25] First, generate a set of "similar" input images by shifting spatially the original image by various small distances. For example, generate nine images: $\mathcal{F}_1, \mathcal{F}_2, \ldots, \mathcal{F}_9$, such that the pixel intensity $v_k^{[x,y]}$ of the kth image at pixel $[x,y]$ is the original intensity of the pixel displaced by $[-r,-s]$, i.e.,

$$v_k^{[x,y]} = w^{[x+r,y+s]}; \quad r,s = -1,0,1; \quad k = 5+r+3s. \qquad \text{(B3)}$$

(Example: $\mathcal{F}_3$ is the original image shifted by $[r,s]=[1,-1]$.) The PC approach yields a linear filter with (3×3) blurring convolution kernel. The elements of the covariance matrix **C** in (34) are autocovariances of the original image. (An attempt to make the PC filter locally sensitive will make it nonstationary.) The filter provides a compromise between the removal of noise and of the deterministic component (information). The degree of this removal can be assessed by viewing the differential image (original image minus filtered image) by the discarded PC images, and by comparison of the eigenvalues, respectively. While being "optimal" in the PC sense—all PCs containing mainly noise and insignificant information are discarded—*it does not require knowledge of the noise spectrum.* Spectral properties of this filter and its relationship to other "optimal" filters (for example, to the Wiener filter) is the subject of our current investigation.

In our experience with spin-echo images of the brain, when the first three out of nine PCs are used, the original pixel contributes about 40%–60% (given by the central element of the kernel) to the filtered pixel value, and when the first six PCs are used, approximately 60%–80% comes from the original pixel. [Noise suppression without a spatial blur may be achieved in image sequences by other transforms as well, usually by extracting "essential information" along the third dimension (e.g., time, image count), and then by applying the corresponding inverse transform to this extracted data. For example, a good noise suppression in gated cardiac studies can be achieved by a low pass Fourier filter.[34] However, from the definition of the PCA, it follows that if a strong deterministic high-frequency component is present in the third dimension, a PC filter may pass it through and provide superior results. As another example, significant noise suppression can also be achieved[22] by the artificial neural network approach.] The situation in radionuclide images is similar. Figure 4 illustrates the filtering effect of the PC filter based on a single image, in this case on the third image of the first row of Fig. 1. The filters based on the first two and on the first four PCs, respectively, suppress significantly the noise (the first two images of the second row of Fig. 4). Because of the character of the image the blur is not easy to notice (which would not be the case with much less noisy MR images). (One may further extend this technique by using 126 images created by shifting all 14 images of the time sequence. We are in the process of evaluating this type of filter.)

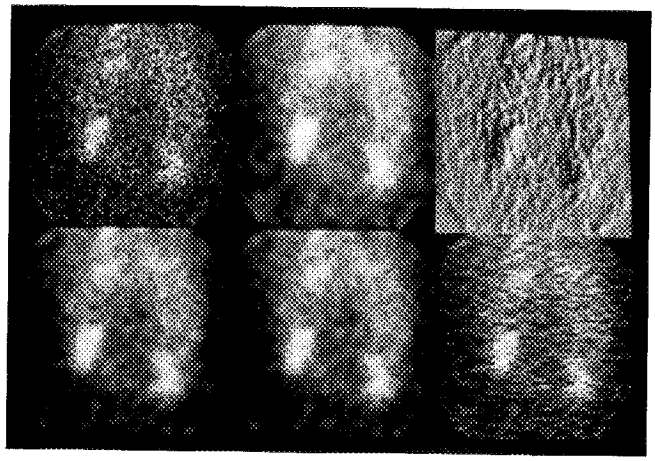

FIG. 4. Nuclear medicine: a planar kidney image. First row: original image, and the first and the second PC images calculated on nine images obtained by shift (see Appendix B). Second row: image filtered by the single-image PC filter based on two, four, and six PCs, respectively.

[1]F. W. Wehrli, J. R. MacFall, G. H. Glover, N. Grigsby, V. Haughton, and J. Johanson, "The dependence of nuclear magnetic resonance (NMR) image contrast on intrinsic and pulse sequence timing parameters," Magn. Res. Imag. **2**, 3–16 (1984).
[2]W. H. Perman, S. K. Hilal, H. E. Simon, and A. A. Maudsley, "Contrast manipulation in NMR imaging," Magn. Res. Imag. **2**, 23–32 (1984).
[3]R. E. Hendrick, "Image contrast and noise," in *Magnetic Resonance Imaging*, edited by D. D. Stark and W. G. Bradley (Mosby, St. Louis, MO, 1988).
[4]F. W. Wehrli, "Principles of magnetic resonance," in Ref. 3, Chap. 1.
[5]R. M. Henkelman, P. Hardy, P. Y. Poon, and M. J. Bronskill, "Optimal pulse sequence for imaging hepatic metastases," Radiology **161**, 727–734 (1986).
[6]P. A. Bottomley, T. H. Foster, E. Raymond, and L. M. Pfeifer, "A review of normal tissue hydrogen NMR relaxation times and relaxation mechanisms from 1–100 MHz: Dependency on tissue type, NMR frequency, temperature, species, excision, and age," Med. Phys. **4**, 11 (1984).
[7]P. A. Bottomley, C. J. Hardy, R. E. Argesinger, and H. A. Allen-Moore, "A review of ^{1}H nuclear magnetic relaxation in pathology: Are T_1 and T_2 diagnostic?," Med. Phys. **1**, 14 (1987).

[8]S. J. Reiderer, S. A. Bobman, J. N. Lee, F. Farzaneh, and H. Z. Wang, "Improved precision in calculated T1 MR images using multiple spin echo acquisition," J. Comput. Assist. Tomogr. **10**, 103–110 (1986).
[9]S. A. Bobman, S. J. Riederer, J. N. Lee, S. A. Suddarth, and H. Z. Wang, "Synthesized MR images: Comparison with acquired images," Radiology **155**, 731–738 (1985).
[10]S. A. Bobman, S. J. Riederer, J. N. Lee, S. A. Suddarth, H. Z. Wang, B. P. Drayer, and J. R. MacFall, "Cerebral magnetic resonance image synthesis," Am. J. Neuro. Rad. **6**, 265–269 (1985).
[11]E. Oja, *Subspace Methods of Pattern Recognition* (Wiley, New York, 1983).
[12]D. A. Ortendahl and N. M. Hylton, "Principal component analysis applied to MRI," in *Book of abstracts: Society of Magnetic Resonance in Medicine 1986,* Berkeley, CA; Soc. of Magn. Resonance Med. **1**, 225–226 (1986).
[13]J. J. Sychra, D. Spigos, D. Pavel, V. Capek, and K. Chan, "Synthetic NMR images with increased information content and decreased noise," *5th Annual Meeting of the Society for Magnetic Resonance Imaging,* San Antonio, TX, February 1987.
[14]J. J. Sychra and V. Capek, "Synthetic NMR images with enhanced information content," *Proceedings of the 14th Congress of the European Society of Neuroradiology,* Udine, Italy, 8–11 September 1987, pp. 341–343.
[15]J. J. Sychra, V. Capek, A. Horowitz, M. Mafee, and K. Chan, "Transformations producing information enhanced MR synthetic images," *The 6th Annual Meeting of the Society of Magnetic Resonance Imaging,* Boston, February, 1988.
[16]W. K. Pratt, *Digital Image Processing* (Wiley, New York, 1978).
[17]D. A. Ortendahl and J. W. Carlson, "Segmentation of MRI images using fuzzy clustering," *Proceedings of the 10th International Conference on Information Processing in Medical Imaging,* Utrecht, 1987.
[18]J. P. Windham, M. A. Abd-Allah, D. A. Reinman, J. W. Froelich, and A. M. Hagar, "Eigenimage filtering in MR imaging," J. Comput. Assist. Tomogr. **3**, 1–9 (1988).
[19]J. J. Sychra, K. Chan, V. Capek, and M. Mafee, "Synthetic MR images with enhanced tissue contrast by supervised pixel intensity subspace methods," SPIE Vol. 1137, Science and Engineering of Medical Imaging, 1989.
[20]J. J. Sychra, K. Chan, V. Capek, M. Mafee, "Synthetic MR images produced by subspace methoeds: A comparison," in *Information Processing in Medical Imaging,* Wiley-Liss, Inc., 1991, pp. 299–312.
[21]J. J. Sychra, D. G. Pavel, and E. Olea, "Radionuclide synthetic Fourier images of cardic wall motion abnormalities," Med. Phys. **16**, Jul/Aug 1989.
[22]J. J. Sychra, "Neural network tools for generation of factor analysis images," IPMI Conference, Kent, England, July 1991.
[23]J. J. Sychra, D. Trepashko, R. Butler, and Q. Lin, "Filters for noise suppression in image sequences," Annual SNM meeting, Cincinnati, June 1991.
[24]R. DiPaola, C. Penel, J. P. Bazin, and C. Berche, "Factor analysis and scintigraphy," in *Information Processing in Scintigraphy,* Proceedings of the 4th International Conference, Orsay, edited by C. Raynaud and A. Todd-Pokropek, ISBN-2-7272-000606, 1975, pp. 91–123.
[25]P. Schmidlin and E. Rosel, in Ref. 24, pp. 80–90.
[26]H. Soltanian-Zadeh, J. P. Windham, and J. M. Jenkins, "Error propagation in eigenimage filtering," IEEE Trans. Med. Imag. **4**, 405–420 (1990).
[27]D. C. Barber and K. S. Nijran, "Factor analysis of dynamic radionuclide studies," in *Information Processing in Medical Imaging,* edited by M. Goris University of Stanford, 1981, pp. 13–28.
[28]F. Cavailloles, J. P. Bazin, and R. DiPaola, "Factor analysis in gated cardiac studies," J. Nucl. Med. **25**, 1067–1079 (1984).
[29]M. M. Tatsuoka, *Multivariate Analysis* (Wiley, New York, 1971).
[30]K. Pearson, "On lines and planes of closest fit to systems of points in space," Philos. Mag. **6**, 559–572 (1901).
[31]M. Karny and M. Samal, "Bayesian rank estimation with application to factor analysis," Kybernetika **26**, 1–12 (1993).
[32]P. Bandettini, A. Jesmanowicz, E. C. Wong, and J. S. Hyde, "Processing strategies for time–course data set in functional MRI of the human brain," Magn. Resonance Med. **30**, 161–173 (1993).